Environmental Science and Pollution Research (2019) 26:25733–25748
https://doi.org/10.1007/s11356-019-05820-9

RESEARCH ARTICLE

High spatial and seasonal heterogeneity of pCO_2 and CO_2 emissions in a karst groundwater-stream continuum, southern China

Junbing Pu[1] · Jianhong Li[1] · Tao Zhang[1] · Xiaofeng Xiong[1] · Daoxian Yuan[1]

Received: 11 February 2019 / Accepted: 24 June 2019 / Published online: 2 July 2019

Abstract

Accurate quantification of the emission of CO_2 from streams and rivers is one of the primary challenges in determining the global carbon budget because our knowledge of the spatial and seasonal heterogeneity on these CO_2 emissions is limited. In karst areas, the groundwater-stream continuum is likely ubiquitous because the carbon-rich groundwater discharges into some of the streams through springs or subterranean streams, which results in more complex spatial and seasonal variations in the CO_2 emissions. To address this issue, the spatial and seasonal characteristics of partial pressure of CO_2 (pCO_2), the $\delta^{13}C_{DIC}$, and the CO_2 emission flux of the Guancun surface stream (GSS) karst groundwater-stream continuum in southern China were investigated from the stream head (groundwater outlet) to the downstream mouth during the 2014–2017 period. Our results reveal that the pCO_2 and CO_2 emissions exhibit high spatial and seasonal heterogeneities over ~1300 m in the GSS. Spatially, the pCO_2 and CO_2 emissions decrease sharply from the stream head (mean 8818.4 μatm for pCO_2 and mean 423.4 mg m^{-2} h^{-1} for CO_2 emission) to the site farthest downstream (mean 2752.7 μatm for pCO_2 and 257.0 mg m^{-2} h^{-1} for CO_2 emission). Except for the dates when extreme rainfall occurred, the pCO_2 and CO_2 emission values were higher in the rainy season than in the dry season. This suggests that in a groundwater-stream continuum, CO_2 emission occurs very soon after the water is transferred from the karst groundwater to the surface water. We estimate that the total amount of CO_2 released to the atmosphere from the GSS is 21.75 t CO_2/year, which is only 1.71–5.62% of the dissolved inorganic carbon loss flux in the GSS during the study period. It is important to note that the measured CO_2 emission and pCO_2 levels decrease farther downstream, so carbon loss is underestimated when it is calculated using downstream sampling points. Therefore, accurate assessments of the CO_2 emission flux need to take into consideration the high spatio-temporal heterogeneity in order to reduce the bias of the entire CO_2 emission flux.

Keywords Spatial and seasonal heterogeneity · Partial pressure of CO_2 · CO_2 emission flux · Karst groundwater-stream continuum · Southern China

Introduction

The latest assessment report points out that the global carbon budget imbalance was + 0.5 Pg C/year on average for 2008–2017 (Le Quéré et al. 2018). Thus, balancing the global carbon budget is still a problem for determining the looping of global carbon (Le Quéré et al. 2018). Recently, inland waters (rivers, streams, reservoirs, and lakes) have been recognized as an important part of the global carbon cycle because they link the terrestrial and marine carbon reservoirs (Cole et al. 2007; Raymond et al. 2013; Regnier et al. 2013; Holgerson and Raymond 2016; Hotchkiss et al. 2018; Tranvik et al. 2018). Carbon dioxide (CO_2) emissions from inland waters may represent a significant CO_2 source to the atmosphere because inland water bodies are often higher CO_2 partial pressure (pCO_2) than atmospheric CO_2 equilibrium. A global estimate of 2.1 Pg C/year of CO_2 emission flux from inland waters has been recently reported (Raymond et al. 2013), which may account for some of the imbalance in the global carbon flux between the different carbon reservoirs (Cole et al. 2007; Battin et al. 2009; Aufdenkampe et al. 2011; Tranvik et al. 2018).

Responsible editor: Philippe Garrigues

✉ Junbing Pu
junbingpu@karst.ac.cn

[1] Key Laboratory of Karst Dynamics, MNR & Guangxi, Institute of Karst Geology, Chinese Academy of Geological Sciences, No. 50, Qixing Ave., Qixing District, Guilin 541004, China

In recent years, the influence of groundwater discharge on CO_2 emissions from inland waters has received significant attention. Groundwater can transport high concentrations of dissolved carbon (inorganic and organic), which originates from biogenic and/or geologic carbon, to the surface and possibly change the carbon balance of the aquatic and surrounding terrestrial ecosystems (Johnson et al. 2008; Oviedo-Vargas et al. 2015; Looman et al. 2016; Oviedo-Vargas et al. 2016; Pu et al. 2017; Duvert et al. 2018). Continental karst water bodies are an important category of inland water bodies on earth because they are typically carbon-rich bodies. Many studies have shown that karst systems play an important role in regulating the regional and global carbon cycles through carbonate mineral dissolution and precipitation (Yuan 1997; Jiang and Yuan 1999; Liu and J. 2000; Martin 2013, 2017; Liu et al. 2018), which is a large fraction of the residual land sink (Le Quéré et al. 2018). In karst areas, many surface streams (headwaters) are only fed by a karst spring or a subterranean stream, which constitutes a groundwater-stream continuum. The carbon-rich nature of karst groundwater results in the high carbon contents of surface streams and the high CO_2 gradient between the water and air, and thus, karst groundwater influences carbon exchange processes. It has been suggested that karst groundwater carrying soil-respired CO_2 may degas some of this CO_2 back into the atmosphere when it is discharged from the karst aquifers (Curl 2012). Several studies have estimated the CO_2 emission flux on certain time-scales and the carbon sink effect in small karst groundwater-stream continuums (de Montety et al. 2011; Jiang et al. 2013; Khadka et al. 2014; Liu et al. 2015; Yang et al. 2015; Pu et al. 2017). Other studies have reported that the pCO_2 and the dissolved inorganic carbon (DIC) of karst groundwater-stream continuums decrease farther downstream because CO_2 is emitted as the water travels away from the high CO_2 sources (Drysdale et al. 2003; Doctor et al. 2008; Wang et al. 2010; de Montety et al. 2011). However, research on the spatial variability of CO_2 emissions from the karst groundwater outlet to the stream mouth is sorely lacking. In particular, few studies have been conducted on the spatial heterogeneity of CO_2 emission longitudinally along a single karst stream.

Accurately quantifying CO_2 emission from a karst groundwater-stream continuum is important for assessing the carbon sink effect because karst systems are being recognized as a key component of the global carbon cycle (Yuan 1997; Larson 2011; Curl 2012; Martin 2017; Liu et al. 2018). The objectives of this study are to confirm the high spatial and seasonal heterogeneity of the pCO_2 and CO_2 emissions of a karst groundwater-stream continuum and to determine how these variations affect the carbon budget of this continuum. This study is based on data collected from a 1300-km typical tropical karst groundwater-stream continuum in southern China. The data collected provide relatively high spatial scale of the variations in CO_2 emissions and contribute to a deeper understanding of dynamic CO_2 processes in karst groundwater-stream continuums. Our results will aid in the accurate upscaling of CO_2 emissions across different karst groundwater-stream continuums and the accurate estimation of the amount of carbon sequestered in karst streams.

Materials and methods

Study area

The Guancun surface stream (GSS) is located in Daliang Town, Rong'an County, Guangxi Zhuang Autonomous Region, China (Fig. 1). The GSS is a typical subtropical headwater stream. It is almost exclusively fed by the Guancun underground stream (GUS) in the upper Devonian (D_{3r}) limestone aquifer since no surface tributaries flow into the GSS (Pu et al. 2017; Pu et al. 2019). The outlet of the GUS is the head of the GSS. Thus, they constitute a typical karst groundwater-surface stream continuum (Fig. 1). The length and average width of the GSS are 1320 m and 3.5 m, respectively. The water level of the GSS is controlled by the GUS discharge and exhibits large fluctuations due to monsoon precipitation (Fig. 2). At base level, the water depth is shallow (0.2–1.2 m).

The study area is in an eastern Asian monsoon climate, so it is characterized by a cold–dry winter from late November through March and a hot–rainy summer from April through October. The annual average air temperature is 19.7 °C and the multi-annual average precipitation is 1726 mm, 72% of which occurs in the wet season from late April to early September. As a typical monsoon region, the air temperature and precipitation in the GSS catchment co-vary, i.e., they are both high in the wet season and low in the dry season (Fig. 2).

In this study, four monitoring sites were chosen along the GSS channel for sampling (Fig. 1). The most upstream site, site GC1 (24° 52′ 10″ N, 109° 20′ 07″ E), is located at the GUS outlet, which is characterized by typical karst groundwater. There were two monitoring sites in the middle of the GSS, site GC2 (24° 51′ 53″ N, 109° 20′ 03″ E) and site GC3 (24° 51′ 45″ N, 109° 20′ 05″ E). The downstream site, site GC4 (24° 51′ 32″ N, 109° 20′ 01″ E), is near the stream mouth, approximately 1.30 km downstream of site GC1. According to our manual field measurements taken in the middle of the channel, the distance from site GC1 to site GC2, site GC2 to site GC3, and site GC3 to site GC4 is 560 m, 276 m, and 456 m, respectively (Fig. 1).

Field sampling and lab analyses

Monthly field measurements were conducted at the four monitoring sites (GC1, GC2, GC3, and GC4) during the 2014–2017 period. Hydrochemical variables, including water temperature

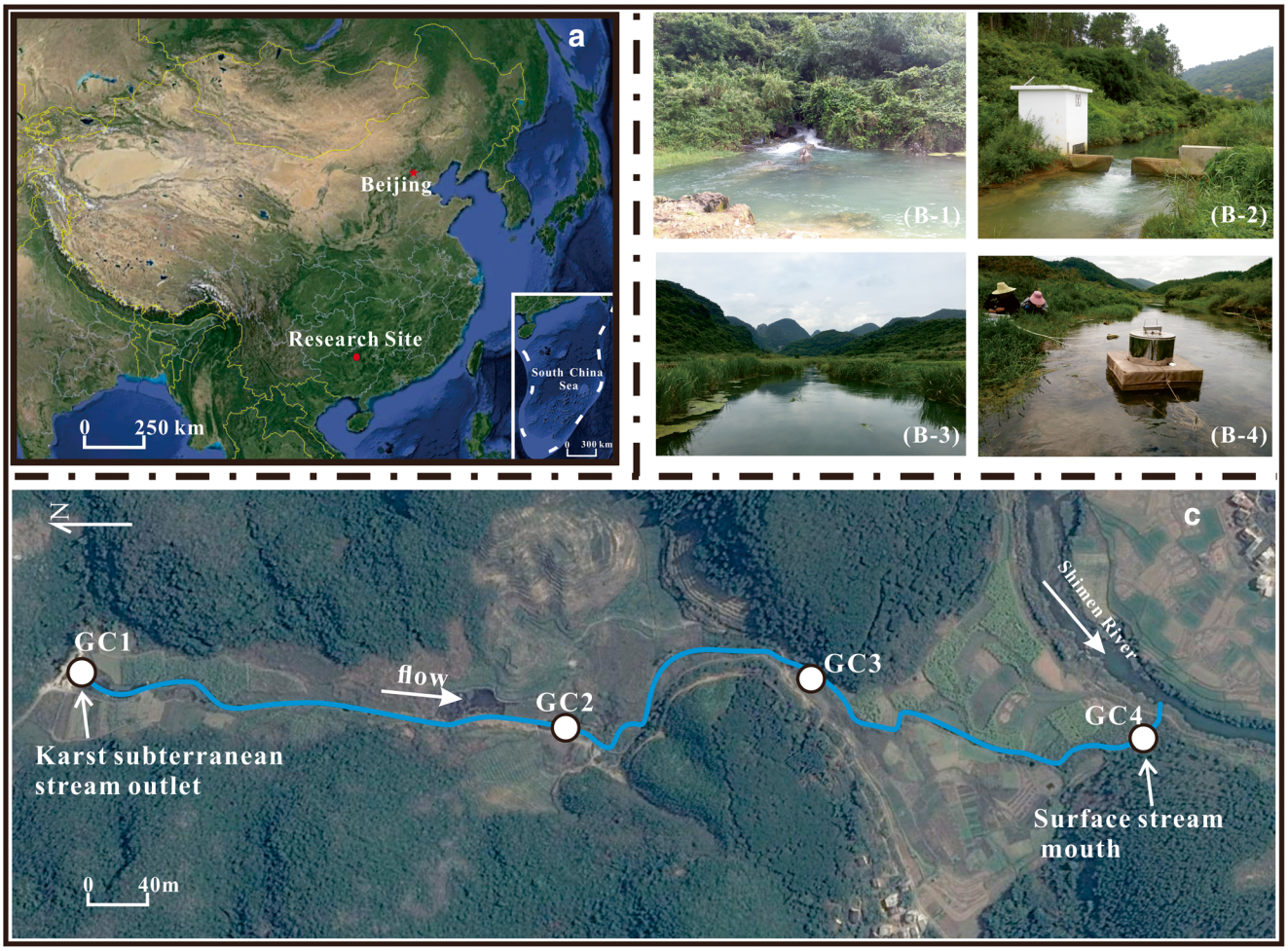

Fig. 1 Study area. **a** Google Earth image of the location of the Guancun Stream in SW China. **b** Photographs showing the landscape of the sample sites, the groundwater outlet (GC1, B-1), the middle of the stream (GC2, B-3 and B-4), and the stream mouth (GC4, B-2), respectively. **c** Map of the surface stream flow route and the sample sites in the study area. (Modified from Google Earth 2015)

(WT), pH, and dissolved oxygen (DO), were tested monthly in situ at the four sites using multi-parameter meters (WTW 3430, WTW GmbH, Weilheim, Germany). The resolutions of the water temperature, pH, and dissolved oxygen (DO) were 0.1 °C, 0.004 pH units, and 0.01 mg/L, respectively. The pH probe was calibrated prior to deployment using pH standards (4 and 7) according to the manufacturer's specifications. The DO probe was calibrated using water saturated air.

Water samples were collected at all four sites from midstream using a peristaltic pump. The water was pumped from 0.1 m below the surface. Unfiltered water samples were immediately titrated to determine the total alkalinity with an accuracy of 0.05 mmol/L using a portable testing kit (Merck KGaA Co., Germany). All of the water samples were immediately filtered through 0.45 μm cellulose acetate membranes for ion analysis and were subsequently stored in acid-washed high-density polyethylene (HDPE) bottles. The samples filtered for cation analysis (Ca^{2+}, Mg^{2+}, K^{+}, and Na^{+}) were acidified with trace-metal grade nitric acid (7 M HNO_3) to a pH of < 2.0. The samples filtered for analysis of the stable carbon isotopes of the dissolved inorganic carbon ($\delta^{13}C_{DIC}$) were collected in acid-washed dry HDPE bottles and three drops of $HgCl_2$ were added in order to prevent microbial activity. A portable cooler was used to store all of the samples in the field. All of the water samples were stored at 4 °C in a refrigerator in the laboratory until they were analyzed.

According to procedures based on the APHA 2012 methods (Rice et al. 2012), the major anions and cations were measured using an automated Dionex ICS-900 ion chromatograph and ICP–OES (IRIS Intrepid II XSP, Thermo Fisher Scientific, USA), respectively. Calculated analytical errors were within ± 5%. The $\delta^{13}C_{DIC}$ values of the water samples were analyzed using a MAT-253 mass spectrometer coupled with a Gas Bench II automated device. The results are expressed as $\delta^{13}C_{DIC}$ (‰) with respect to the Vienna Pee Dee Belemnite (V-PDB) standard with an analytical precision of ± 0.15‰. All of the lab analyses were conducted in the Environmental and Geochemical Analysis Laboratory at the Institute of Karst Geology, Chinese Academy of Geological Science (Pu et al. 2017; Zhang et al. 2017).

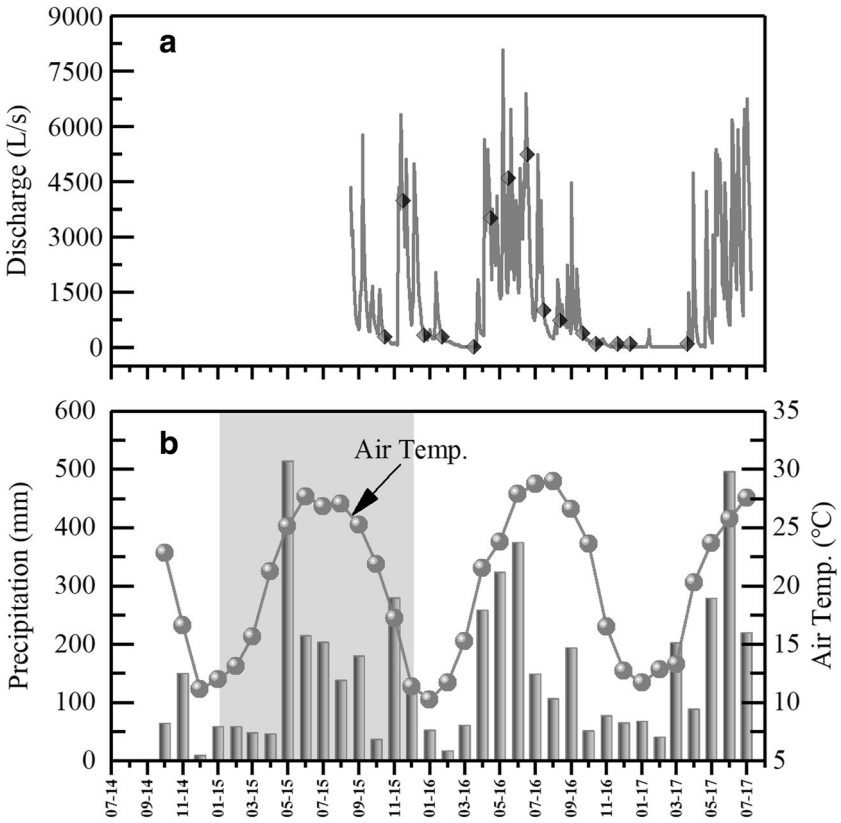

Fig. 2 Variation in the hydro-meteorological parameter. **a** Variations in the daily discharge of the GSS from August 18, 2015 to July 9, 2017. **b** Variations in the monthly cumulative precipitation and the monthly average air temperature from July, 2014 to July, 2017. The black diamonds in Fig. 2a are partial sampling trips during the study period. The gray-shaded area shows the extreme El Niño year in 2015 (Ma and Ye 2016)

The rainfall and air temperature were measured using an on-site Vantage Pro 2 weather station (Davis Instruments Corp., USA) during the study period. The resolutions of the rainfall and air temperature were 0.2 mm and 0.1 °C, respectively. Continuous hydrological monitoring started on August 18, 2015, which have 10 months lag compared to the hydrochemical monitoring (Fig. 2a). The daily discharge of the GSS from August 18, 2015 to July 9, 2017 was obtained from the water-level measurements at the gauging station and the water-level-discharge formula.

The CO_2SYS program, which is based on the measured alkalinity, pH, and water temperature, was used to calculate the aqueous partial pressure of CO_2 (pCO_2) and the inorganic carbon species including HCO_3^-, dissolved CO_2, and CO_3^{2-} using the carbonic acid dissociation constants and the CO_2 solubility (Lewis and Wallace 2006). The DIC concentration was calculated using the formula $DIC = H_2CO_3 + HCO_3^- + CO_3^{2-}$. The CO_2SYS software is commonly used to obtain the pCO_2 and inorganic carbon species in freshwater and seawater (Butman and Raymond 2011; Ran et al. 2015b; Ran et al. 2017b; Deirmendjian and Abril 2018; Li et al. 2018a).

CO_2 evasion flux monitoring

The floating chamber method (FC) was employed to study the CO_2 evasion flux across the water–air interface (Fig. 1). The floating chamber is a very popular and relatively low-cost instrument that can determine the diffusive flux at the surface of aquatic ecosystems (Matthews et al. 2003; UNESCO/IHA GHG 2010; Khadka et al. 2014; Lorke et al. 2015). A home-made floating chamber with a volume of ~ 28.3 L and a surface area of 0.0707 m^2 was constructed from a polyurethane foam layer sandwiched between two stainless steel cylinders. About 5 cm of the chamber is placed under water and the level is maintained using a styrofoam sheet. At each site, a floating chamber was placed at midstream in the GSS. Prior to deployment, the chambers were placed upside down for a few minutes to allow them to equilibrate with the local air. The air samples were drawn from the chamber via a Tygon tube after deployment using an aspirator pump. The gas samples were stored in a Devex polymer-aluminum bag (volume 1 L) at room temperature. The gas samples were analyzed for CO_2 concentration within 48 h of collection using gas chromatography (Agilent-7890) with a resolution of 0.01 ppmv. The five concentrations collected at ~ 0, 5, 10, 15, and 30 min enabled us to calculate the CO_2 flux using linear regression. Only sites with a correlation coefficient higher than 0.90 for CO_2 were used.

The flux was calculated using the equation (UNESCO/IHA GHG 2010): CO_2 flux (mg m^{-2} h^{-1}) = $(S \times F_1 \times F_2 \times V)/(Sf \times F_3)$, where S is the slope from graph of concentration versus time in ppm/min, F_1 is the conversion factor from ppm to μg/m^3 (1798.45 for CO_2), F_2 is the conversion factor from minutes to hour (60), V is the volume of air trapped in the

chamber (m^3), Sf is the surface of the floating chamber over the water (m^2), and F_3 is the conversion factor from μg to mg (1000).

Results

Hydro-meteorological characteristic

During the monitoring period (August, 18, 2015–July 9, 2017), the GSS discharge ranges from 6.1 to 8069.4 L/s with an average value of 1295.5 L/s and a high coefficient of variation of 128.3% (Fig. 2a). Generally, the GSS discharge increased following precipitation with a relatively short lag time. The GSS was dominantly recharged by karst groundwater from the GUS and mirrored the hydrological variation of the GUS karst aquifer. A significant seasonal variation in the discharge of the GSS was observed during the study period, with a higher discharge in the rainy season and a lower discharge in the dry season, which is consistent with the monsoon climate of the study area. In 2015, an abnormal flood event occurred in the GSS in November and December, 2015 due to abnormal precipitation events caused by extreme El Niño effects (Ma and Ye 2016) (Fig. 2a). In 2016–2017, the GSS had a normal hydrological curve with two higher discharge events in April–July and late August–early October and two low discharge periods in January–March and August (Fig. 2a).

During the study period, the average monthly air temperature in the GSS area ranged from 10.3 to 29.0 °C with the higher value occurring in summer and the lower value in winter (Fig. 2a). The monthly precipitation ranged from 8.9 to 513.4 mm (Fig. 2a). Generally, more precipitation occurred in the summer than in the winter due to the Asian monsoon climate. In 2015, an extreme El Niño event impacted the study area and resulted in extreme precipitation events. The total yearly precipitation was 1903 mm in 2015 with the highest value occurring in May 2015 (513.4 mm) and the second highest occurring in November 2015 (278.8 mm).

Variability of the WT, pH, DO, inorganic carbon species, and $\delta^{13}C_{DIC}$

The water temperature (WT) varied from 14.8 to 24.9 °C in the GSS. The WT of site GC1 is inherited from the GUS karst aquifer, ranging from 19.0 to 21.7 °C with a low coefficient of variation (CV) of 3.35%. The WT increased from site GC1 to site GC4. The downstream sites GC2, GC3, and GC4 had relatively high CVs of 7.09%, 10.27%, and 12.42%, respectively (Table 1, Fig. 3) and were likely affected by the ambient air temperature. The pH of the water ranged from 7.223 to 8.281 in the GSS. A gradual increase in pH occurred from site GC1 to site GC4 during the study period (Table 1, Fig. 3). The highest average pH value occurred at site GC4 (8.025), while the lowest occurred at site GC1 (7.504). The DO concentration varied from 6.14 to 16.72 mg/L during the study period. The lowest DO value was observed at site GC1. The other three sites, GC2, GC3, and GC4, had higher DO concentrations and larger variation ranges than those of site GC1 (Table 1).

The inorganic carbon species were primarily DIC, HCO_3^-, and dissolved CO_2 (Rice et al. 2012). Site GC1 had the highest DIC, HCO_3^-, and dissolved CO_2 concentration, which varied from 180.38 to 348.02 mg/L, from 2789.71 to 5091.10 μmol/L, and from 154.04 to 657.50 μmol/L, respectively, throughout the study period due to recharge from karst groundwater. The DIC, HCO_3^-, and dissolved CO_2 decreased downstream from site GC1 to site GC4, demonstrating significant spatial variation ($p < 0.01$ by ANOVA) (Table 1). Since the pH value ranged from 7.223 to 8.281 in the GSS, HCO_3^- was the dominant component of the DIC in all of the water samples from the GSS, accounting for 93.0%, 95.9%, 97.2%, and 97.4% of the DIC on average for sites GC1, GC2, GC3, and GC4, respectively.

The $\delta^{13}C_{DIC}$ values ranged from − 14.44 to − 9.53‰ (mean = − 12.82‰) at site GC1 and were lower than those of the downstream sites ($p < 0.05$ by ANOVA) (Table 1). Generally, the mean $\delta^{13}C_{DIC}$ value increased from site GC1 to site GC2 (Fig. 3). The lowest mean $\delta^{13}C_{DIC}$ values occurred at site GC1, which was directly impacted by karst groundwater. The $\delta^{13}C_{DIC}$ values of site GC2 ranged from − 16.61 to − 9.05‰ (mean = − 12.29‰). The highest mean $\delta^{13}C_{DIC}$ values (mean = − 11.94‰) occurred at site GC3 ranging from − 14.45 to − 9.03‰. The $\delta^{13}C_{DIC}$ values of site GC4 ranged from − 16.07 to − 9.55‰ with a mean of − 12.05‰.

pCO_2 and CO_2 emission variability

All of the water samples had pCO_2 values higher than the atmospheric value (~ 420 μatm) and were supersaturated with CO_2 (Table 1). The pCO_2 of site GC1 had the highest mean value (8818.4 μatm) and ranged from 4073.8 to 16,595.9 μatm. pCO_2 decreased significantly from site GC1 to site GC4 ($p < 0.01$ by ANOVA) (Fig. 3). The mean pCO_2 values of sites GC2, GC3, and GC4 were 3817.3 μatm, 2732.9 μatm, and 2752.7 μatm, respectively.

The CO_2 emission flux varied significantly from 16.5 to 1125.3 mg m^{-2} h^{-1} during the study period. Site GC1 had the largest mean CO_2 emission flux (423.4 mg m^{-2} h^{-1}) and ranged from 35.7 to 950.0 mg m^{-2} h^{-1}, which is about 26 times fluctuation. A significant decrease in the total CO_2 emission flux occurred from site GC1 to site GC2 ($p < 0.01$ by ANOVA). The mean CO_2 emission flux decreased from 411.1 mg m^{-2} h^{-1} at site GC2 to 328.4 mg m^{-2} h^{-1} at site GC3 to 257.0 mg m^{-2} h^{-1} at site GC4. The amplitude of the variations in the CO_2 emission flux at sites GC2, GC3, and GC4 were significantly lower than that of site GC1.

Table 1 Summary of the statistics of the DIC species, water temperature, pH, dissolved oxygen, SIc, pCO_2, $\delta^{13}C_{DIC}$, and the CO_2 flux at the four sites along the GSS

Monitoring periods			HCO_3^-	CO_2	DIC	Water temp.	pH	DO	SIc	pCO_2	$\delta^{13}C_{DIC}$	CO_2 flux
			μmol/L	μmol/L	mg/L	°C		mg/L		μatm	‰	mg m^{-2} h^{-1}
GC1	October, 2014~July, 2017	Mean	4694.41	353.76	308.72	20.58	7.504	7.71	0.35	8818.4	− 12.82	423.4
		Median	4736.25	354.80	311.50	20.80	7.498	7.61	0.38	8709.6	− 13.19	375.1
		Minimum	2789.71	154.04	180.38	19.00	7.223	6.14	− 0.16	4073.8	− 14.44	35.7
		Maximum	5091.10	657.50	348.02	21.70	7.813	8.87	0.70	16,595.9	− 9.53	950.0
		S.D.[a]	429.40	135.76	31.47	0.69	0.154	0.77	0.17	3208.7	1.25	263.9
		C.V.[b]	9.15	38.38	10.19	3.35	2.048	10.02	47.66	36.4		62.3
		N[c]	28	28	28	28	28	28	27	27	26	27
GC2	October, 2014~July, 2017	Mean	4601.67	159.41	292.85	21.10	7.834	10.76	0.66	3817.3	− 12.29	411.1
		Median	4674.44	135.15	298.53	21.38	7.865	10.38	0.71	3311.3	− 12.27	384.6
		Minimum	2486.51	90.32	158.11	17.80	7.550	7.98	− 0.03	2238.7	− 16.61	76.5
		Maximum	4980.22	300.49	330.15	24.20	8.060	16.72	0.98	7585.8	− 9.05	851.2
		S.D.[a]	462.13	60.48	30.22	1.50	0.146	2.26	0.26	1354.5	1.41	295.8
		C.V.[b]	10.04	37.94	10.32	7.09	1.868	20.96	39.04	35.5		72.0
		N[c]	28	28	28	28	28	25	28	28	28	17
CC3	October, 2014~March, 2017	Mean	4520.02	111.44	283.84	21.20	7.972	9.11	0.80	2732.8	− 11.94	328.4
		Median	4562.93	107.87	286.40	21.60	7.978	9.38	0.83	2511.39	− 11.99	251.8
		Minimum	2533.01	59.79	159.98	16.30	7.711	0.87	0.24	1513.6	− 14.45	38.7
		Maximum	5051.73	190.93	316.41	24.10	8.180	10.85	1.05	4786.3	− 9.03	1125.3
		S.D.[a]	454.77	33.98	28.59	2.18	0.120	1.83	0.20	837.5	1.26	274.8
		C.V.[b]	10.06	30.49	10.07	10.27	1.505	20.07	24.59	30.6		83.7
		N[c]	27	27	27	27	27	26	27	27	27	16
GC4	October, 2014~July, 2017	Mean	4559.99	99.36	285.71	21.12	8.025	9.16	0.76	2752.7	− 12.05	257.0
		Median	4634.58	92.82	289.17	21.80	8.043	9.40	0.86	2454.7	− 11.95	254.6
		Minimum	2985.45	53.52	190.63	14.80	7.710	7.37	0.01	1548.8	− 16.07	16.5
		Maximum	5163.26	160.60	325.50	24.90	8.281	10.45	1.01	6166.0	− 9.55	844.2
		S.D.[a]	380.04	28.54	23.43	2.62	0.128	0.78	0.28	930.4	1.27	260.6
		C.V.[b]	8.33	28.72	8.20	12.42	1.599	8.51	37.29	33.8		101.4
		N[c]	28	28	28	28	28	27	28	28	27	27

[a] *S.D.*, standard deviation

[b] C.V. (coefficient of variation) = (standard deviation/mean) × 100, C.V. is not reported for $\delta^{13}C_{DIC}$ values as these can be negative

[c] *N*, the amount of sample or data

Discussion

High seasonal and spatial heterogeneity of the pCO_2 and CO_2 emission flux

We determined that the pCO_2 and CO_2 emission flux of the GSS had a high seasonal heterogeneity (Fig. 3). Generally, the pCO_2 fluctuated from 1513.6 μatm (at site GC3) in the dry season to 16,595.9 μatm (at site GC1) in the rainy season. The mean pCO_2 values were the highest at site GC1 in both seasons, whereas the lowest value was observed at site GC3. Higher pCO_2 values were observed in the rainy season than in the dry season at all of the sites except for site GC1 (Fig. 3, Table 1). Soil CO_2 input, respiration of organic carbon, and CO_2 influx from the ambient air above the surface stream will increase the amount of CO_2 and the pCO_2, while in-stream photosynthesis and CO_2 emission from the water to the ambient air will decrease pCO_2 (Wallin et al. 2013; Peter et al. 2014; Marx et al. 2017; Pu et al. 2017; Deirmendjian and Abril 2018). The pCO_2 of site GC1 is impacted by the karst aquifer because it is the outlet of the GUS. During the rainy season, greater amounts of soil CO_2 are produced by strong organic carbon degradation flows into the karst aquifer, resulting in an increase in the pCO_2 of the groundwater, which has been reported in numerous studies of subtropical karst areas in southern China (Yang et al. 2012; Pu et al. 2014; Zhao et al. 2015). However, hydrological processes likely disturb this trend

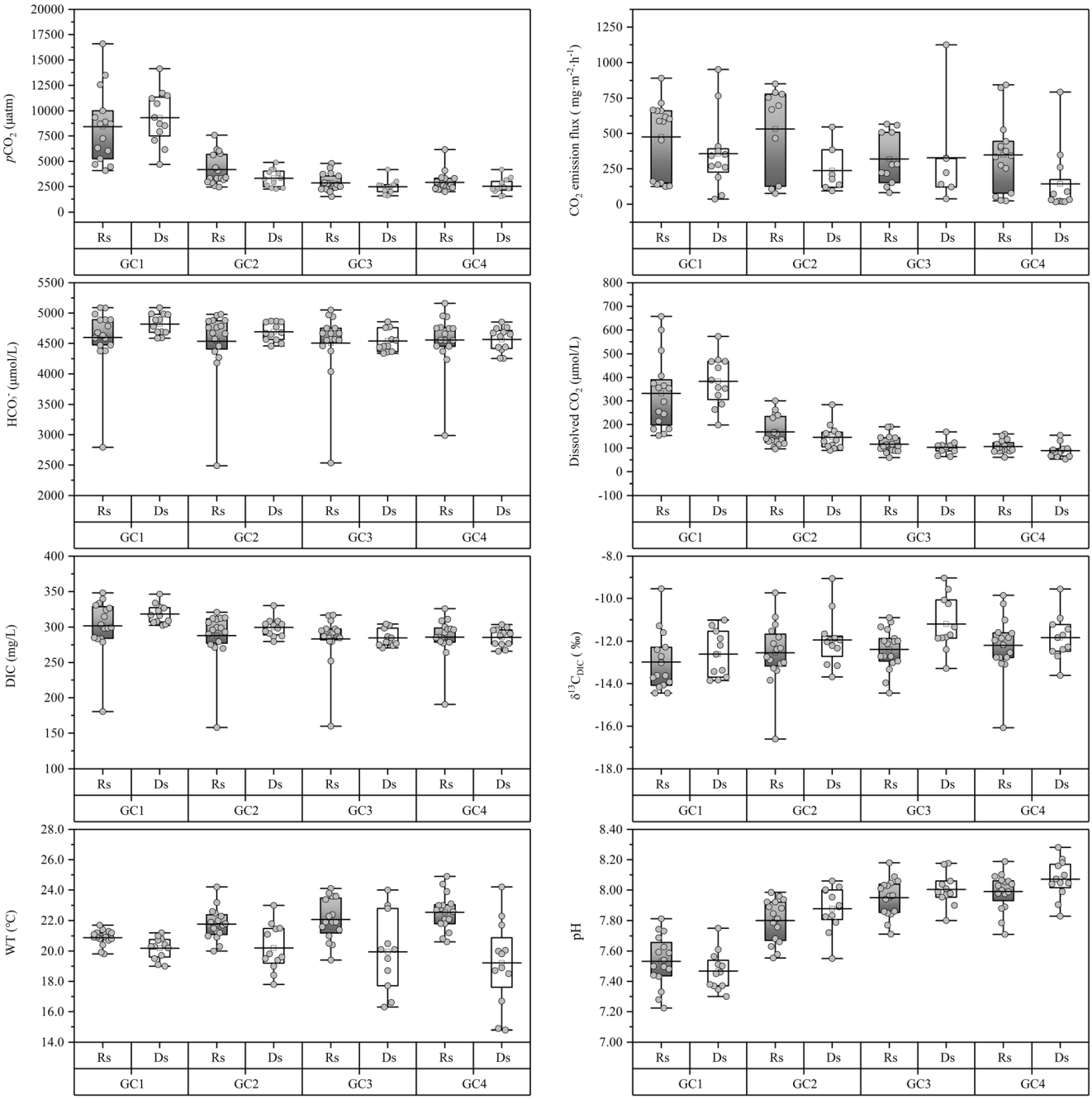

Fig. 3 Spatio-temporal heterogeneity of the DIC species, pCO_2, $\delta^{13}C_{DIC}$, CO_2 emission flux, water temperature (WT), and pH from 2014 to 2017 in the GSS. Box plots of the 25th and 75th percentiles and mean values; whiskers represent minimum and maximum values. The Rs and the Ds represent the rainy season and the dry season, respectively

(Sun et al. 2007; Yao et al. 2007; Peter et al. 2014; Almeida et al. 2017). During the rainy season, a lot of surface water carrying less soil CO_2 flows directly into the aquifer through sinkholes, fractures, fissures, or shafts, which could significantly dilute the karst groundwater and decrease the pCO_2 level (Liu et al. 2007; Pu et al. 2014; van Geldern et al. 2015; Marx et al. 2017). The good Pearson correlation coefficient ($r = -0.80$, $p < 0.05$, Table 2) between the discharge and pCO_2 values of site GC1 during rainy season indicates that discharge has an impact on the variation of pCO_2. This also results in a larger range and lower mean value of the pCO_2, HCO_3^- concentration, dissolved CO_2 content, DIC concentration, and $\delta^{13}C_{DIC}$ values and a higher mean pH (Fig. 3, Table 2). During the dry season, due to the low air temperature and low discharge in the study area, although soil CO_2 recharge was low, the GUS discharge significantly decreased, which resulted in a relative high mean pCO_2 at site GC1.

The downstream sites (GC2, GC3, and GC4) had higher pCO_2 values in the rainy season than in the dry season

Table 2 Pearson correlation coefficients between discharge, pCO_2, CO_2 emission flux, and selected variables (significance levels: $p < 0.05$)

			Water discharge	CO_2 emission flux	pCO_2	DIC	$\delta^{13}C_{DIC}$	HCO_3^-	CO_2	WT	pH	DO
GC1 site	Rainy season	Water discharge	1.00									
		CO2 emission flux	0.65	1.00								
		pCO_2	−0.80	−0.54	1.00							
		DIC	−0.86	−0.59	0.72	1.00						
		$\delta^{13}C_{DIC}$	0.02	0.19	−0.19	−0.37	1.00					
		HCO_3^-	−0.88	−0.56	0.58	0.98	−0.34	1.00				
		CO_2	−0.77	−0.51	1.00	0.73	−0.36	0.58	1.00			
		WT	−0.75	−0.18	0.42	−0.11	0.36	−0.22	0.32	1.00		
		pH	0.85	0.47	−0.96	−0.57	0.37	−0.41	−0.96	−0.40	1.00	
		DO	0.86	0.54	−0.79	−0.65	0.27	−0.55	−0.80	−0.54	0.79	1.00
	Dry season	Water discharge	1.00									
		CO2 emission flux	0.94	1.00								
		pCO_2	−0.23	−0.23	1.00							
		DIC	−0.57	−0.54	0.64	1.00						
		$\delta^{13}C_{DIC}$	−0.29	0.15	0.00	−0.40	1.00					
		HCO_3^-	−0.73	−0.54	0.21	0.88	−0.50	1.00				
		CO_2	−0.26	−0.26	1.00	0.65	−0.01	0.22	1.00			
		WT	−0.18	−0.27	0.09	−0.07	−0.10	−0.14	0.07	1.00		
		pH	0.16	0.11	−0.97	−0.47	−0.16	−0.01	−0.97	0.02	1.00	
		DO	0.24	0.32	0.07	−0.20	0.38	−0.30	0.08	−0.75	−0.24	1.00
GC2 site	Rainy season	Water discharge	1.00									
		CO2 emission flux	0.66	1.00								
		pCO_2	−0.13	0.12	1.00							
		DIC	−0.74	−0.34	0.43	1.00						
		$\delta^{13}C_{DIC}$	−0.39	−0.31	−0.18	−0.23	1.00					
		HCO_3^-	−0.78	−0.39	0.34	1.00	−0.22	1.00				
		CO_2	−0.18	0.06	0.99	0.44	−0.21	0.35	1.00			
		WT	−0.59	−0.08	−0.14	0.09	0.57	0.11	−0.15	1.00		
		pH	−0.02	−0.17	−0.91	−0.04	0.15	0.05	−0.91	0.23	1.00	
		DO	−0.26	0.30	−0.29	0.27	0.34	0.31	−0.31	0.78	0.49	1.00
	Dry season	Water discharge	1.00									
		CO2 emission flux	0.81	1.00								
		pCO_2	0.79	0.53	1.00							
		DIC	−0.09	0.20	0.51	1.00						
		$\delta^{13}C_{DIC}$	0.24	0.16	−0.08	0.26	1.00					
		HCO_3^-	−0.28	0.07	0.09	0.32	−0.62	1.00				
		CO_2	0.78	0.52	0.83	0.78	0.38	−0.15	1.00			
		WT	−0.05	−0.23	−0.16	−0.13	0.11	−0.50	−0.01	1.00		
		pH	−0.74	−0.43	−0.89	−0.71	−0.31	0.15	−0.99	0.03	1.00	
		DO	−0.91	−0.57	−0.26	0.40	0.75	−0.50	0.29	0.49	−0.19	1.00
GC3 site	Rainy season	Water discharge	1.00									
		CO2 emission flux	0.44	1.00								
		pCO_2	0.29	−0.03	1.00							
		DIC	−0.56	−0.67	0.34	1.00						
		$\delta^{13}C_{DIC}$	−0.92	−0.30	−0.18	−0.06	1.00					
		HCO_3^-	−0.61	−0.67	0.29	1.00	−0.05	1.00				
		CO_2	0.17	−0.17	0.99	0.38	−0.12	0.33	1.00			
		WT	−0.28	−0.46	−0.12	−0.06	0.45	−0.06	−0.13	1.00		
		pH	−0.35	−0.01	−0.88	0.08	0.21	0.13	−0.87	0.19	1.00	

Table 2 (continued)

			Water discharge	CO_2 emission flux	pCO_2	DIC	$\delta^{13}C_{DIC}$	HCO_3^-	CO_2	WT	pH	DO
		DO	−0.38	0.51	−0.20	0.48	0.14	0.50	−0.21	0.09	0.41	1.00
	Dry season	Water discharge	1.00									
		CO2 emission flux	0.98	1.00								
		pCO_2	0.84	0.77	1.00							
		DIC	0.51	0.54	0.61	1.00						
		$\delta^{13}C_{DIC}$	−0.56	−0.63	−0.56	−0.25	1.00					
		HCO_3^-	0.42	0.46	0.53	1.00	−0.20	1.00				
		CO_2	0.83	0.77	0.99	0.64	−0.54	0.56	1.00			
		WT	−0.01	−0.02	−0.24	−0.43	−0.12	−0.42	−0.34	1.00		
		pH	−0.71	−0.65	−0.96	−0.53	0.50	−0.45	−0.97	0.42	1.00	
		DO	−0.21	−0.07	−0.32	−0.19	0.69	−0.16	−0.29	−0.26	0.25	1.00
GC4 site	Rainy season	Water discharge	1.00									
		CO2 emission flux	0.56	1.00								
		pCO_2	0.29	0.64	1.00							
		DIC	−0.73	−0.16	0.04	1.00						
		$\delta^{13}C_{DIC}$	−0.44	0.11	0.25	−0.12	1.00					
		HCO_3^-	−0.74	−0.18	0.01	1.00	−0.12	1.00				
		CO_2	0.13	0.46	0.65	0.01	−0.12	−0.04	1.00			
		WT	−0.49	0.23	0.34	−0.04	0.59	−0.04	0.00	1.00		
		pH	−0.46	−0.46	−0.51	0.41	0.09	0.45	−0.90	0.03	1.00	
		DO	0.31	−0.32	−0.13	0.35	−0.17	0.36	−0.15	−0.35	0.26	1.00
	Dry season	Water discharge	1.00									
		CO2 emission flux	0.90	1.00								
		pCO_2	0.51	0.13	1.00							
		DIC	0.39	0.56	0.32	1.00						
		$\delta^{13}C_{DIC}$	−0.78	−0.60	−0.36	−0.85	1.00					
		HCO_3^-	0.36	0.53	0.29	0.99	−0.85	1.00				
		CO_2	0.43	0.47	0.39	0.40	−0.36	0.30	1.00			
		WT	0.07	0.01	−0.40	−0.13	−0.08	−0.14	−0.06	1.00		
		pH	−0.44	−0.43	−0.33	−0.23	0.17	−0.13	−0.97	0.10	1.00	
		DO	0.02	−0.20	0.03	−0.33	0.34	−0.29	−0.34	−0.43	0.20	1.00

($p < 0.05$ by ANOVA). This phenomenon was directly controlled by the soil CO_2 influx and the in-stream respiration/decomposition of organic matter. As was previously mentioned, a lot of soil CO_2 could flow into the GUS along with the rainwater and increase the pCO_2 value of the stream (Yang et al. 2012; Marx et al. 2017; Campeau et al. 2018). In addition, a higher water temperature and stronger solar radiation can promote in situ respiration and produce more CO_2 in the stream (Marx et al. 2017). Thus, the pCO_2 level increased in the GSS during the rainy season. This process was also observed in several large subtropical rivers: the lower Red River (Le et al. 2018), the Xijiang River (Yao et al. 2007), and the Guijiang River (Zhang et al. 2017). Due to the influence of the soil CO_2 influx and the respiration of organic matter on the pCO_2 values of the GSS, elevated discharge played a minor role at sites GC2, GC3, and GC4 (Table 2).

CO_2 emission flux varied seasonally, ranging from 16.5 mg m^{-2} h^{-1} at site GC4 in the dry season to 1125.3 mg m^{-2} h^{-1} at site GC3 in the dry season. However, the mean CO_2 emission flux exhibits a regular pattern characterized by higher values during the rainy season and lower values during the dry season at all four of the sites along the GSS (Fig. 3). Usually, the CO_2 emission flux is controlled by hydrological processes (lotic or lentic water) and the CO_2 concentration gradient between the water and the ambient air (Raymond et al. 2013; Long et al. 2015; Gomez-Gener et al. 2016; Looman et al. 2016; Marx et al. 2017). Generally, the air pCO_2 is approximately 445 μatm 1.5 m above the stream surface and changes slightly throughout the year (Pu et al. 2017). Our data indicate that the mean water pCO_2 of the water was about 6–21 times higher than that of the ambient air. Thus, the higher water pCO_2 levels during the rainy season

Table 3 Comparison of our data with the results of previous studies pCO_2 and CO_2 emission flux studies in different climate conditions (S, summer; W, winter; A, autumn; D, dry season; We, wet season)

River or stream	Sites	Climate zone	Time period	Mean precipitation mm	Mean air temp.	Mean CO_2 evasion flux mmol m^{-2} day^{-1}	Mean pCO_2 μatm	k600 cm/h	Reference
Guancun GC1	China	Subtropic	2014~2017	1726	19.7	230.9	8818.4		This study
Guancun GC2	China	Subtropic	2014~2017	1726	19.7	224.2	3817.3		This study
Guancun GC3	China	Subtropic	2014~2017	1726	19.7	179.1	2732.8		This study
Guancun GC4	China	Subtropic	2014~2017	1726	19.7	140.2	2752.7		This study
Guijiang (upstream DM)	China	Subtropic	2016	1666	20	− 11.3 (S), 0.3 (W)	366 (S), 422 (W)	5.8 (S), 3.9 (W)	Zhang et al. (2017)
Guijiang (downstream PY)	China	Subtropic	2016	1666	20	26 (S), − 10 (W)	1236 (S), 179 (W)	5.7(S), 4.5(W)	Zhang et al.(2017)
Xijiang	China	Subtropic	2005~2006		14–22	189.0~356.2	2600	8~15	Yao et al. (2007)
Zambezi River	Africa	Subtropic	2012~2013	1400		281.7	2475~3730	2.7	Teodoru et al. (2015)
Santa Fe River	USA	Subtropic	2010~2012	1195	20.4	92~264	10,790		Khadka et al. (2014)
Daning River	China	Subtropic	2016~2017	1124.5	17.5	329.8	1198.2		Ni et al. (2019)
Yangtze River (Datong station)	China	Subtropic	1960s~2000			14~54	1297	8	Wang et al. (2007)
Yangtze River (Three Gorges Reservoir)—main stream	China	Subtropic	2016–2017	1250	15~19	212.5 (Jun.), 79.6 (Nov.), 76.3 (Mar.), 123.3 (Jul.)	2104.7 (Jun.), 2826.0 (Nov.), 2774.6 (Mar.), 2345.7 (Jul.)	14.6 (Jun.), 3.4 (Nov.), 3.3 (Mar.), 7.0 (Jul.)	Li (2018)
Yangtze River (Three Gorges Reservoir)—tributaries	China	Subtropic	2015–2016	1250	15~19	350 (D), 326 (W)	1573 (D), 1276 (W)	30.8 (D), 45.6 (W)	Li et al. (2018b)
Yellow River (main stream)	China	Temperate	2013–2014			661.9 (D), 886.2 (We)	3687	26.7 (D), 47.2 (We)	Ran et al. (2015a)
Buffalo Bayou	USA	Subtropic	2008			326.5	3052	2.59–4.18	Zeng and Masiello (2010)
Spring Creek	USA	Subtropic	2008			533.4	4702	2.31–3.78	Zeng and Masiello (2010)
Lower Mekong River	–	Tropic	1972~1998	–	–	194.5	1090	26	Li et al. (2013)
Amazon	Brazil	Tropic	1995~1996	–	–	189.0	4350	10	Richey et al. (2002)
Amazon	Brazil	Tropic	2004~2007	–	–	345.2	3320	15	Alin et al. (2011)
Tigris	Turkey	Continental	2008~2009	611.1–294.1	14.6–21.8	107.7	1277		Varol and Li (2017)
Hudson	USA	Temperate	1992~1995	–	–	16.1	1125	1.54	Raymond et al. (1997)
Mississippi River	USA	Temperate	1972–2001			269.9	1335	16.3	Dubois et al. (2010)
Wuding River	China	Temperate	2015	300–500		172 (S), 116 (S), 218 (A)	425–2499	29–36.8	Ran et al. (2017a)

are favorable to CO_2 evasion due to the large CO_2 concentration gradient between the water and the ambient air. The elevated discharge in the rainy season could change the hydraulic status and disturb the surface water, which would accelerate the emission of CO_2 (Long et al. 2015; Looman et al. 2016; Almeida et al. 2017). This is supported by the good Pearson correlation coefficient between the discharge and the CO_2 emission flux (Table 2). It is notable that there were several high CO_2 emission events during the dry season (Fig. 3), and some of these events approached or exceeded the highest values for the rainy season. We determined that these high values occurred in November, 2015 during a rare flood event caused by extreme precipitation (278.8 mm) due to El Niño (Fig. 2). This flood changed the hydrological status and stimulated CO_2 emission, which resulted in the higher values.

This study demonstrates that the high spatial heterogeneity of the pCO_2 and CO_2 emission can occur within a distance of only ~ 1300 m of stream. Generally, a clear decrease in pCO_2 occurred from site GC1 to site GC4 in both the rainy and dry seasons ($p < 0.05$ by ANOVA). The rate of decrease of pCO_2 was 9.63 μatm/m from site GC1 to site GC2, 2.89 μatm/m from site GC2 to site GC3, and 0.12 μatm/m from site GC3 to site GC4, illustrating the complex spatial variability of the GSS. Although the total mean CO_2 emission flux decreased significantly from site GC1 downstream to site GC4 (Table 1), different patterns of change were observed for the rainy and dry seasons. In the rainy season, no significant changes in the CO_2 emission flux occurred from site GC1 to site GC2 ($p = 0.590$ by ANOVA) or from site GC3 to site GC4 ($p = 0.856$ by ANOVA). Significant changes in the CO_2 emission flux only occurred from site GC2 to site GC3 ($p < 0.05$ by ANOVA) during the rainy season. In the dry season, except for the anomaly high value in November, 2015, the CO_2 emission flux changed significantly from site GC1 to site GC2 ($p < 0.05$ by ANOVA), from site GC2 site to site GC3 ($p < 0.05$ by ANOVA), and from site GC3 to site GC4 ($p < 0.05$ by ANOVA). Thus, the CO_2 emission flux of the GSS exhibits a complex spatial variability in different seasons.

The decrease in pCO_2 from site GC1 to GC4 is most likely controlled by two processes: (1) assimilation of CO_2 by aquatic plants during photosynthesis and (2) the emission of CO_2 (Marx et al. 2017). The sharp decrease in pCO_2 from site GC1 to site GC2 was likely caused by a large amount of CO_2 emission coupled with the high water discharge of the rainy season (Fig. 3). Usually, the DO content can be used as a proxy of the intensity of in-stream photosynthesis (Demars et al. 2015; Pu et al. 2017). Significant in-stream photosynthesis in the GSS has been reported by a previous study (Pu et al. 2017). Therefore, during the rainy season, an increase in the mean DO value from site GC1 (mean 7.77 mg/L) to site GC2 (mean 10.10 mg/L) (Table 1) implies that the photosynthesis of the aquatic plants in the GSS assimilates the CO_2 and DIC in the water and releases DO into the water (Demars et al. 2015), which also decreases the pCO_2 level. During the dry season, the significant decrease in the pCO_2 level in the GSS from site GC1 to site GC2 was also caused by a large amount of CO_2 emission and the use of CO_2 and DIC in in-stream photosynthesis, which the mean DO value increased from 7.63 to 11.73 mg/L (Fig. 3). An increase in the amount of photosynthesis and CO_2 emission from site GC1 to site GC2 likely caused increases in pH and $\delta^{13}C_{DIC}$ and decreases in the HCO_3^-, dissolved CO_2, and DIC contents (Fig. 3). After strong CO_2 occurred at sites GC1 and GC2, stream pCO_2 reached a relatively low level. Hence, CO_2 emissions at site GC3 and GC4 were far low than at site GC2 during the rainy and dry seasons (Fig. 3). The smaller difference in the pCO_2 values of sites GC3 and GC4 resulted in smaller difference in their CO_2 emission fluxes (Fig. 3).

Numerous previous studies have concluded that many large rivers exhibit significant spatial and seasonal variability in pCO_2 and CO_2 emissions as a result of changes in the channel, lake or reservoir control, metropolitan influences, and special climate conditions (Yao et al. 2007; Li et al. 2013; Raymond et al. 2013; Ran et al. 2015a; Ran et al. 2015b; Almeida et al. 2017; Ran et al. 2017b; Wang et al. 2017; Zhang et al. 2017; Le et al. 2018). In addition, several studies have determined that CO_2-rich groundwater recharge along the channel at the headwater of the system or into forest creeks likely causes significantly spatial and seasonal variability in the pCO_2 and CO_2 emissions (Kokic et al. 2015; Looman et al. 2016; Schelker et al. 2016; Marx et al. 2017; Deirmendjian and Abril 2018; Duvert et al. 2018). Our results reveal that pronounced spatial and seasonal variability of pCO_2 and CO_2 emission flux also occurred within ~ 1300 m of a small karst groundwater-stream continuum, with a 68.8% decrease in the mean pCO_2 from site GC1 (groundwater outlet) to site GC4 (farthest downstream). In particular, in the first 560 m, the mean pCO_2 decreased by 56% from site GC1 to site GC2, which accounts for 81.4% of the total decrease. The high spatial variability is consistent with the findings of several previous studies. Venkiteswaran et al. (2014) pointed out that most of the CO_2 originating from groundwater is lost by emission within a short distance, causing pCO_2 to decrease sharply. Johnson et al. (2008) found that in Amazonian headwater streams, over 90% of the CO_2 was emitted within 20 m downstream of a groundwater seepage area. Öquist et al. (2009) found that in a Swedish boreal catchment, 65% of the DIC export to the stream was emitted to the atmosphere as CO_2 within 200 m of the groundwater entering the stream. Duvert et al. (2018) compiled spatially groundwater-derived pCO_2 data for 15 streams and creeks in tropical, temperate, and boreal areas and determined that the quantity of CO_2 dissolved in the water decreased by 64 to > 92% (median 76%) in the first 100 m downstream of the groundwater outflow area. These findings suggest that CO_2 emission in a groundwater-stream continuum occurs very soon after the

groundwater enters the surface stream. Therefore, this study highlights the fact that the measured CO_2 emission and pCO_2 levels decrease along the length of streams and C loss is underestimated when it is calculated from the concentrations of downstream sampling points. Thus, high temporal-spatial resolution sampling along a groundwater-stream continuum is required to constrain the CO_2 water dynamics.

Magnitude of CO_2 evasion in the GSS

The pCO_2 and CO_2 emission flux of the GSS is comparable to the values observed in other streams and rivers in tropical, subtropical, temperate, and continental climates (Table 3). Due to the high spatial variability of the CO_2 emission flux observed in this study, we separated the four monitoring sites into two groups: the upstream sites (sites GC1 and GC2) and the downstream sites (sites GC3 and GC4). Generally, the pCO_2 values of the upstream sites were significantly higher than most of the values reported for major rivers in Asia, i.e., Yellow River's main stream (3687 μatm), the Yangtze River (1297–2826 μatm), and the Lower Mekong River (1090 μatm), as well as other rivers around the world such as the Amazon (3230 μatm or 4350 μatm) and Zambezi (2475–3730 μatm) Rivers. These values also significantly exceed those of several subtropical rivers, i.e., the Guijiang, Daning, and Xijiang Rivers and most temperate and continental rivers, i.e., the Mississippi, Hudson, Wuding, and Tigris (Table 3). The pCO_2 values of the downstream sites had higher values (> 2500 μatm), which also exceeded those of several subtropical rivers, i.e., the Yangtze, Guijiang, Daning, Xijiang, and Lower Mekong Rivers, and several temperate rivers, i.e., the Mississippi, Hudson, and Wuding Rivers (Table 3). The pCO_2 values of the vast majority of the rivers and streams listed were higher than that of atmospheric CO_2 equilibrium (Table 3), suggesting that these rivers and streams are oversaturated in CO_2 and act as CO_2 sources to the atmosphere. Our estimated CO_2 emission fluxes for the upstream sites are fall within the middle of the previously reported range of flux (Table 3). However, the estimated CO_2 emission fluxes of the downstream sites fall within the lower end of the published rates (< 200 mmol m^{-2} day^{-1}) (Table 3). A subtropical river, the Guijiang River, has a negative CO_2 flux in the summer and winter, implying that the river directly absorbs ambient atmospheric CO_2 and is a carbon sink (Table 3). However, the CO_2 emissions of all of the sites along the GSS were positive. The highest CO_2 emission flux was found in the main stream of the Yellow River (886.2 and 661.9 mmol m^{-2} day^{-1} for the rainy and the dry seasons, respectively). Temperate rivers (Mississippi River), subtropical rivers (Daning and Zambezi River), tropical river (Amazon River), and subtropical stream (Buffalo Bayou and Spring Creek) tend to have CO_2 emission flux 1.1–1.5 times higher than the upstream sites and CO_2 emission fluxes 1.5–2.3 times higher than the downstream sites in the GSS (Table 3). In general, although the GSS is a small karst stream with a ~ 1300 m length, its CO_2 emission flux is comparable to that of some large rivers due to the local enrichment of karst groundwater with high CO_2 or DIC concentrations.

CO_2 emission flux and the DIC flux of the stream

The discharge, CO_2 emission, and DIC data of the four sites from October 2015 to December 2016 were used to calculate the CO_2 emission flux and the DIC flux of the stream. The distance between two neighboring sample sites was manually measured in the field at midstream. The surface area of the stream was estimated by mapping each stream sector between two sample sites using the polygon applications in Google Earth Pro. Then, each sector was multiplied by the corresponding average flux of the two neighboring sample sites and the results were added together to calculate the overall CO_2 emission flux (t CO_2/year) (Teodoru et al. 2015). The average annual dissolved inorganic carbon (F_{DIC}) fluxes of the different sectors of the GSS were calculated from the mean annual discharge (Q_m), the instantaneous DIC concentrations (DIC_i), and the instantaneous discharge rates (Q_i) (Brunet et al. 2009) using the following equation: $F_{DIC} = 365 Q_m \left[\frac{\sum_{i=1}^{n} DIC_i Q_i}{\sum_{i=1}^{n} Q_i} \right]$. Since the GSS is a karst groundwater-fed stream with a short stream channel, this study assumes that the discharge does not significantly change from site GC1 to site GC4, i.e., within the length studied. Thus, the same instantaneous discharge was used for all four of the sites in each monitoring period to calculate the DIC flux.

The calculated results indicate that the total amount of CO_2 released into the atmosphere from the GSS was 21.75 t CO_2/year. This value is equal to the sum of the three sectors, i.e., 13.16 t CO_2/year from site GC1 to site GC2, 3.62 t CO_2/year from site GC2 to site GC3 and 4.97 t CO_2/year from site GC3 to site GC3. The calculated DIC yield from the GC1 site was 1.24×10^4 t DIC/year, which represented DIC export from the GUS karst system. The calculated DIC fluxes of sites GC2, GC3, and GC4 are 1.17×10^4 t DIC/year, 1.15×10^4 t DIC/year, and 1.14×10^4 t DIC/year, respectively, showing a decreasing trend due to carbon loss through CO_2 emission, carbon assimilation by aquatic phototrophs, or/and calcite precipitation in the GSS (Pu et al. 2017). In this study, we calculated the approximate carbon loss between two neighboring sample sites. The DIC loss flux was 0.07×10^4 t DIC/year from site GC1 to site GC2, 0.02×10^4 t DIC/year from site GC2 to site GC3, and 0.01×10^4 t DIC/year from site GC3 to site GC4. Thus, the carbon loss ratio due to CO_2 emission (CO_2 emission flux/DIC loss flux) was 1.17% from site GC1 to site GC2, 2.96% from site GC2 to site GC3, and 5.62% from site GC3 to

site GC4. Overall, the CO_2 emission flux from the GSS only accounts for 1.71–5.62% (mean = 3.43%) of the stream's DIC loss flux, which falls within the lower end of the range of published ratios (2–30%; Liu et al. 2010). The estimated CO_2 emission ratio indicates that the proportion of CO_2 lost from the GSS was low, implying that most of the DIC loss was the result of carbon assimilation by aquatic phototrophs or/and calcite precipitation, which is consistent with the results of Pu et al. (2017).

Further implications

Demonstrating the high spatio-temporal heterogeneity of pCO_2 and CO_2 emissions contributes to our understanding of carbon cycle processes and to improving the accuracy of the carbon budget in karst catchments. Although several new techniques and methods, e.g., high-resolution online monitoring equipment, floating autochambers, and thin boundary layer models, were used to study the CO_2 emissions from streams and rivers, accurately estimating of the CO_2 emission flux is still difficult due to high spatio-temporal heterogeneities. This study provides a new point of view regarding the complexity of the spatio-temporal variations of CO_2 emission in a karst groundwater-stream continuum. The obvious seasonal heterogeneity of the pCO_2 and CO_2 emission flux implies that monitoring should be conducted over as many seasons as possible, and should at least include the dry and rainy seasons. Specially, the pCO_2 and CO_2 emission flux of some extreme climate events should be taken into account. If sampling was conducted during the dry season, a low pCO_2 value and CO_2 emission flux would be obtained, whereas if sampling was conducted during the rainy season, the annual CO_2 emission could be overestimated. If sampling was conducted during or immediately after extreme rainfall events, abnormal pCO_2 and CO_2 emission value would be obtained, resulting in the overestimation of the CO_2 emission flux. Complex spatial heterogeneity significantly affects the accuracy of CO_2 emission estimates in karst catchments. The upstream pCO_2 value and CO_2 emission values, especially near the karst groundwater outlet, are significant higher than the downstream values. If sampling is conducted near the karst groundwater outlet, the pCO_2 and CO_2 emission values will be overestimated, whereas, if sampling is conducted downstream, the pCO_2 and CO_2 emission values will be underestimated. Therefore, based on the results of our study, in a groundwater-stream continuum, monitoring sites employing the floating chamber method should be located in the upstream, midstream, and downstream areas. This will provide a relatively accurately estimate of the CO_2 emission flux and allow for the accurate determination of the carbon budget of a groundwater-stream continuum. Therefore, when designing a sampling campaign for a stream or river, it is necessary to include as many time points and sampling sites as possible to accurately calculate the CO_2 emission flux, rather than sampling once at only a few or one sampling site.

Recently, several studies have concluded that since land karst system are carbon sinks, it is uncertain if degassing of from rivers and streams (especially the headwater of the system) can be ignored (Cole et al. 2007; Aufdenkampe et al. 2011; Curl 2012; Marx et al. 2017). In terms of a karst groundwater-stream continuum, the results of our study of the Guancun stream provide important information that sheds light on how regional karst groundwater influences CO_2 emissions from streams on the spatio-temporal scale and increases our understanding of the C source/sink status of karst systems. The Guancun stream is not a unique case, given that the hydrogeological factors (karst groundwater-stream continuum) cause the high CO_2 emission flux on the spatio-temporal scale. In karst areas, streams such as the Guancun stream may represent relatively common hotspots of CO_2 emission, and thus, their emission fluxes merit a closer investigation. In addition, the proportion of CO_2 returned to the atmosphere from the GSS was low, implying that the inorganic carbon exported from the karst system was not fully returned to the atmosphere by groundwater-stream continuum in the form of CO_2 gas and some of the inorganic carbon was fixed by aquatic phototrophs. Overall, the accurate assessment of the CO_2 emission flux in a karst groundwater-stream continuum needs to take into consideration the high spatio-temporal heterogeneity in order to reduce the bias of the CO_2 emission flux and to improve the catchment CO_2 budget balance.

Conclusions

Quantifying the CO_2 emission flux from a stream or river is important to the global carbon balance. However, the high spatial and seasonal heterogeneity of pCO_2 and CO2 emissions restricts the accuracy of quantifying the CO_2 emission flux. This study demonstrates that several physio-chemical parameters, such as pCO_2 and CO_2 emissions, exhibit high spatial and seasonal heterogeneity within a distance of only ~ 1300 m in a small karst groundwater-stream continuum. A significant decrease in the pCO_2 and CO_2 emissions occurred from site GC1 (mean 8818.4 μatm for pCO_2 and mean 423.4 mg m^{-2} h^{-1} for CO_2 emission) to site GC4 (mean 2752.7 μatm for pCO_2 and 257.0 mg m^{-2} h^{-1} for CO_2 emission). Except during extreme rainfall events, higher pCO_2 and CO_2 emission values were observed in the rainy season than in the dry season at most sites. The calculated results show that the total CO_2 released to the atmosphere from the GSS was 21.75 t CO_2/year, which accounts for 1.71–5.62% (mean 3.43%) of the stream's DIC loss flux. Thus, this study highlights the importance of considering spatio-temporal heterogeneities when assessing the CO_2 emission flux from a stream

or river, especially in a groundwater-stream continuum. This study also provides a sampling and monitoring framework that can reduce the potential biases of CO_2 emission assessments.

Acknowledgments Special thanks are given to Dr. Wen Liu, M.Sc. Xue Mo, M.Sc. Li Li, and M.Sc. Feihong Wu for their help in field and lab works.

Funding The study is financially supported by the National Natural Science Foundation of China (No. 41572234, No. 41702271, No. 41202185), the Guangxi Natural Science Foundation (2016GXNSFCA380002, 2017GXNSFFA198006), the Special Fund for Basic Scientific Research of Chinese Academy of Geological Sciences (YYWF201636), and the Geological Survey Project of CGS (DD20160305-03).

Compliance with ethical standards

Conflict of interest The authors declare that they have no conflict of interest.

References

Alin SR, Rasera MFFL, Salimon CI, Richey JE, Holtgrieve GW, Krusche AV, Snidvongs A (2011) Physical controls on carbon dioxide transfer velocity and flux in low-gradient river systems and implications for regional carbon budgets. JGR 116. https://doi.org/10.1029/2010jg001398

Almeida RM, Pacheco FS, Barros N, Rosi E, Roland F (2017) Extreme floods increase CO_2 outgassing from a large Amazonian river. Limnol Oceanogr 62:989–999. https://doi.org/10.1002/lno.10480

Aufdenkampe AK, Mayorga E, Raymond PA, Melack JM, Doney SC, Alin SR, Aalto RE, Yoo K (2011) Riverine coupling of biogeochemical cycles between land, oceans, and atmosphere. Front Ecol Environ 9:53–60. https://doi.org/10.1890/100014

Battin TJ, Luyssaert S, Kaplan LA, Aufdenkampe AK, Richter A, Tranvik LJ (2009) The boundless carbon cycle. Nat Geosci 2:598–600. https://doi.org/10.1038/ngeo618

Brunet F, Dubois K, Veizer J, Nkoue Ndondo GR, Ndam Ngoupayou JR, Boeglin JL, Probst JL (2009) Terrestrial and fluvial carbon fluxes in a tropical watershed: Nyong basin, Cameroon. ChGeo 265:563–572. https://doi.org/10.1016/j.chemgeo.2009.05.020

Butman D, Raymond PA (2011) Significant efflux of carbon dioxide from streams and rivers in the United States. Nat Geosci 4:839–842. https://doi.org/10.1038/ngeo1294

Campeau A, Bishop K, Nilsson MB, Klemedtsson L, Laudon H, Leith FI, Öquist M, Wallin MB (2018) Stable carbon isotopes reveal soil-stream DIC linkages in contrasting headwater catchments. J Geophys Res Biogeosci 123:149–167. https://doi.org/10.1002/2017jg004083

Cole JJ, Prairie YT, Caraco NF, McDowell WH, Tranvik LJ, Striegl RG, Duarte CM, Kortelainen P et al (2007) Plumbing the global carbon cycle: integrating inland waters into the terrestrial carbon budget. Ecosystems 10:172–185. https://doi.org/10.1007/s10021-006-9013-8

Curl RL (2012) Carbon shifted but not sequestered. Sci 335:655

de Montety V, Martin JB, Cohen MJ, Foster C, Kurz MJ (2011) Influence of diel biogeochemical cycles on carbonate equilibrium in a karst river. ChGeo 283:31–43. https://doi.org/10.1016/j.chemgeo.2010.12.025

Deirmendjian L, Abril G (2018) Carbon dioxide degassing at the groundwater-stream-atmosphere interface: isotopic equilibration and hydrological mass balance in a sandy watershed. J Hydrol 558:129–143. https://doi.org/10.1016/j.jhydrol.2018.01.003

Demars BOL, Thompson J, Manson JR (2015) Stream metabolism and the open diel oxygen method: principles, practice, and perspectives. Limnol Oceanogr Methods 13:356–374. https://doi.org/10.1002/lom3.10030

Doctor DH, Kendall C, Sebestyen SD, Shanley JB, Ote N, Boyer EW (2008) Carbon isotope fractionation of dissolved inorganic carbon (DIC) due to outgassing of carbon dioxide from a headwater stream. HyPr 22:2410–2423. https://doi.org/10.1002/hyp.6833

Drysdale R, Lucas S, Carthew K (2003) The influence of diurnal temperatures on the hydrochemistry of a tufa-depositing stream. HyPr 17:3421–3441. https://doi.org/10.1002/hyp.1301

Dubois KD, Lee D, Veizer J (2010) Isotopic constraints on alkalinity, dissolved organic carbon, and atmospheric carbon dioxide fluxes in the Mississippi River. Journal of Geophysical Research: Biogeosciences 115:n/a-n/a https://doi.org/10.1029/2009jg001102

Duvert C, Butman DE, Marx A, Ribolzi O, Hutley LB (2018) CO_2 evasion along streams driven by groundwater inputs and geomorphic controls. Nat Geosci 11:813–818. https://doi.org/10.1038/s41561-018-0245-y

Gomez-Gener L, von Schiller D, Marce R, Arroita M, Casas-Ruiz JP, Staehr PA, Acuna V, Sabater S et al (2016) Low contribution of internal metabolism to carbon dioxide emissions along lotic and lentic environments of a Mediterranean fluvial network. J Geophys Res Biogeosci 121:3030–3044. https://doi.org/10.1002/2016jg003549

Holgerson MA, Raymond PA (2016) Large contribution to inland water CO_2 and CH_4 emissions from very small ponds. Nat Geosci 9:222–226. https://doi.org/10.1038/ngeo2654

Hotchkiss ER, Sadro S, Hanson PC (2018) Toward a more integrative perspective on carbon metabolism across lentic and lotic inland waters. Limnol Oceanogr Lett 3:57–63. https://doi.org/10.1002/lol2.10081

Jiang Y, Hu Y, Schirmer M (2013) Biogeochemical controls on daily cycling of hydrochemistry and $\delta^{13}C$ of dissolved inorganic carbon in a karst spring-fed pool. J Hydrol 478:157–168. https://doi.org/10.1016/j.jhydrol.2012.12.001

Jiang Z, Yuan D (1999) CO_2 source-sink in karst processes in karst areas of China. Episodes 22

Johnson MS, Lehmann J, Riha SJ, Krusche AV, Richey JE, Ometto JPHB, Couto EG (2008) CO_2 efflux from Amazonian headwater streams represents a significant fate for deep soil respiration. GeoRL 35. https://doi.org/10.1029/2008gl034619

Khadka MB, Martin JB, Jin J (2014) Transport of dissolved carbon and CO_2 degassing from a river system in a mixed silicate and carbonate catchment. J Hydrol 513:391–402. https://doi.org/10.1016/j.jhydrol.2014.03.070

Kokic J, Wallin MB, Chmiel HE, Denfeld BA, Sobek S (2015) Carbon dioxide evasion from headwater systems strongly contributes to the total export of carbon from a small boreal lake catchment. J Geophys Res Biogeosci 120:13–28. https://doi.org/10.1002/2014jg002706

Larson C (2011) Climate change: an unsung carbon sink. Sci 334:886–887. https://doi.org/10.1126/science.334.6058.886-b

Le Quéré C, Andrew RM, Friedlingstein P, Sitch S, Hauck J, Pongratz J, Pickers PA, Korsbakken JI et al. (2018) Global carbon budget 2018. Earth Syst. Sci. Data 10:2141–2194 doi:https://doi.org/10.5194/essd-10-2141-2018

Le TPQ, Marchand C, Ho CT, Le ND, Duong TT, Lu X, Doan PK, Nguyen TK et al (2018) CO_2 partial pressure and CO_2 emission along the lower Red River (Vietnam). BGeo 15:4799–4814. https://doi.org/10.5194/bg-15-4799-2018

Lewis DE, Wallace DWR (2006) MS excel program developed for CO_2 system calculations. ORNL/CDIAC-105a. Carbon Dioxide

Information Analysis Center, Oak Ridge National Laboratory, U.S. Department of Energy, Oak Ridge, Tennessee. https://doi.org/10.3334/CDIAC/otg.CO2SYS_XLS_CDIAC105a

Li S (2018) CO_2 oversaturation and degassing using chambers and a new gas transfer velocity model from the Three Gorges Reservoir surface. Sci Total Environ 640-641:908–920. https://doi.org/10.1016/j.scitotenv.2018.05.345

Li S, Bush RT, Santos IR, Zhang Q, Song K, Mao R, Wen Z, Lu XX (2018a) Large greenhouse gases emissions from China's lakes and reservoirs. Water Res 147:13–24. https://doi.org/10.1016/j.watres.2018.09.053

Li S, Lu XX, Bush RT (2013) CO_2 partial pressure and CO_2 emission in the Lower Mekong River. J Hydrol 504:40–56. https://doi.org/10.1016/j.jhydrol.2013.09.024

Li S, Ni M, Mao R, Bush RT (2018b) Riverine CO_2 supersaturation and outgassing in a subtropical monsoonal mountainous area (Three Gorges Reservoir Region) of China. J Hydrol 558:460–469. https://doi.org/10.1016/j.jhydrol.2018.01.057

Liu H, Liu Z, Macpherson GL, Yang R, Chen B, Sun H (2015) Diurnal hydrochemical variations in a karst spring and two ponds, Maolan Karst Experimental Site, China: biological pump effects. J Hydrol 522:407–417. https://doi.org/10.1016/j.jhydrol.2015.01.011

Liu Z, Dreybrodt W, Wang H (2010) A new direction in effective accounting for the atmospheric CO_2 budget: considering the combined action of carbonate dissolution, the global water cycle and photosynthetic uptake of DIC by aquatic organisms. Earth-Sci Rev 99:162–172. https://doi.org/10.1016/j.earscirev.2010.03.001

Liu Z, J. Z (2000) Contribution of carbonate rock weathering to the atmospheric CO_2 sink. Environ. Geol. 39:1053–1058

Liu Z, Li Q, Sun H, Wang J (2007) Seasonal, diurnal and storm-scale hydrochemical variations of typical epikarst springs in subtropical karst areas of SW China: soil CO_2 and dilution effects. J Hydrol 337:207–223. https://doi.org/10.1016/j.jhydrol.2007.01.034

Liu Z, Macpherson GL, Groves C, Martin JB, Yuan D, Zeng S (2018) Large and active CO_2 uptake by coupled carbonate weathering. Earth-Sci Rev 182:42–49. https://doi.org/10.1016/j.earscirev.2018.05.007

Long H, Vihermaa L, Waldron S, Hoey T, Quemin S, Newton J (2015) Hydraulics are a first-order control on CO_2 efflux from fluvial systems. J Geophys Res Biogeosci 120:1912–1922. https://doi.org/10.1002/2015jg002955

Looman A, Santos IR, Tait DR, Webb JR, Sullivan CA, Maher DT (2016) Carbon cycling and exports over diel and flood-recovery timescales in a subtropical rainforest headwater stream. Sci Total Environ 550:645–657. https://doi.org/10.1016/j.scitotenv.2016.01.082

Lorke A, Bodmer P, Noss C, Alshboul Z, Koschorreck M, Somlai-Haase C, Bastviken D, Flury S, McGinnis DF, Maeck A, Müller D, Premke K (2015) Technical note: drifting versus anchored flux chambers for measuring greenhouse gas emissions from running waters. BGeo 12:7013–7024. https://doi.org/10.5194/bg-12-7013-2015

Ma F, Ye A Contribution of the 2015–2016 El Niño on Floods and Droughts in China. In: AGU Fall Meeting, San Francisco, 2016. AGU, p A43C0237M

Martin JB (2013) Do carbonate karst terrains affect the global carbon cycle? Acta Carsologica 42:187–196

Martin JB (2017) Carbonate minerals in the global carbon cycle. ChGeo 449:58–72. https://doi.org/10.1016/j.chemgeo.2016.11.029

Marx A, Dusek J, Jankovec J, Sanda M, Vogel T, van Geldern R, Hartmann J, Barth JAC (2017) A review of CO_2 and associated carbon dynamics in headwater streams: a global perspective. RvGeo 55:560–585. https://doi.org/10.1002/2016rg000547

Matthews CJD, St Louis VL, Hesslein RH (2003) Comparison of three techniques used to measure diffusive gas exchange from sheltered aquatic surfaces. Environ Sci Technol 37:772–780. https://doi.org/10.1021/es0205838

Ni M, Li S, Luo J, Lu X (2019) CO_2 partial pressure and CO_2 degassing in the Daning River of the upper Yangtze River, China. J Hydrol 569:483–494. https://doi.org/10.1016/j.jhydrol.2018.12.017

Öquist MG, Wallin M, Seibert J, Bishop K, Laudon H (2009) Dissolved inorganic carbon export across the soil/stream interface and its fate in a boreal headwater stream. Environ Sci Technol 43:7364–7369

Oviedo-Vargas D, Dierick D, Genereux DP, Oberbauer SF (2016) Chamber measurements of high CO_2 emissions from a rainforest stream receiving old C-rich regional groundwater. Biogeochemistry 130:69–83. https://doi.org/10.1007/s10533-016-0243-3

Oviedo-Vargas D, Genereux DP, Dierick D, Oberbauer SF (2015) The effect of regional groundwater on carbon dioxide and methane emissions from a lowland rainforest stream in Costa Rica. J Geophys Res Biogeosci 120:2579–2595. https://doi.org/10.1002/2015jg003009

Peter H, Singer GA, Preiler C, Chifflard P, Steniczka G, Battin TJ (2014) Scales and drivers of temporal pCO_2 dynamics in an Alpine stream. J Geophys Res Biogeosci 119:1078–1091. https://doi.org/10.1002/2013jg002552

Pu J, Li J, Khadka MB, Martin JB, Zhang T, Yu S, Yuan D (2017) In-stream metabolism and atmospheric carbon sequestration in a groundwater-fed karst stream. Sci Total Environ 579:1343–1355. https://doi.org/10.1016/j.scitotenv.2016.11.132

Pu J, Li J, Zhang T, Martin JB, Khadka MB, Yuan D (2019) Diel-scale variation of dissolved inorganic carbon during a rainfall event in a small karst stream in southern China. Environ Sci Pollut Res 26:11029–11041. https://doi.org/10.1007/s11356-019-04456-z

Pu J, Yuan D, Zhao H, Shen L (2014) Hydrochemical and PCO_2 variations of a cave stream in a subtropical karst area, Chongqing, SW China: piston effects, dilution effects, soil CO_2 and buffer effects. Environ Earth Sci 71:4039–4049

Ran L, Li L, Tian M, Yang X, Yu R, Zhao J, Wang L, Lu XX (2017a) Riverine CO_2 emissions in the Wuding River catchment on the Loess Plateau: environmental controls and dam impoundment impact. J Geophys Res Biogeosci 122:1439–1455. https://doi.org/10.1002/2016jg003713

Ran L, Lu XX, Richey JE, Sun H, Han J, Yu R, Liao S, Yi Q (2015a) Long-term spatial and temporal variation of CO_2 partial pressure in the Yellow River, China. BGeo 12:921–932. https://doi.org/10.5194/bg-12-921-2015

Ran L, Lu XX, Yang H, Li L, Yu R, Sun H, Han J (2015b) CO_2 outgassing from the Yellow River network and its implications for riverine carbon cycle. J Geophys Res Biogeosci 120:1334–1347. https://doi.org/10.1002/2015jg002982

Ran LS, Lu XX, Liu SD (2017b) Dynamics of riverine CO2 in the Yangtze River fluvial network and their implications for carbon evasion. BGeo 14:2183–2198. https://doi.org/10.5194/bg-14-2183-2017

Raymond PA, Caraco NF, Cole JJ (1997) Carbon dioxide concentration and atmospheric flux in the Hudson River. Estuaries 20:381–390

Raymond PA, Hartmann J, Lauerwald R, Sobek S, McDonald C, Hoover M, Butman D, Striegl R, Mayorga E, Humborg C, Kortelainen P, Dürr H, Meybeck M, Ciais P, Guth P (2013) Global carbon dioxide emissions from inland waters. Natur 503:355–359. https://doi.org/10.1038/nature12760

Regnier P, Friedlingstein P, Ciais P, Mackenzie FT, Gruber N, Janssens IA, Laruelle GG, Lauerwald R, Luyssaert S, Andersson AJ, Arndt S, Arnosti C, Borges AV, Dale AW, Gallego-Sala A, Goddéris Y, Goossens N, Hartmann J, Heinze C, Ilyina T, Joos F, LaRowe DE, Leifeld J, Meysman FJR, Munhoven G, Raymond PA, Spahni R, Suntharalingam P, Thullner M (2013) Anthropogenic perturbation of the carbon fluxes from land to ocean. Nat Geosci 6:597–607. https://doi.org/10.1038/ngeo1830

Rice EW, Baird RB, Eaton AD, Clesceri LS (2012) Standard methods for the examination of water and wastewater. 22nd ed. American Public

Health Association, The American Water Works Association and the Water Environment Federation, Washington D.C.

Richey JE, Melack JM, Aufdenkampe AK, Ballester VM, Hess LL (2002) Outgassing from Amazonian rivers and wetland as a large tropical source of atmospheric CO_2. Natur 416:617–620

Schelker J, Singer GA, Ulseth AJ, Hengsberger S, Battin TJ (2016) CO_2 evasion from a steep, high gradient stream network: importance of seasonal and diurnal variation in aquatic pCO_2 and gas transfer. Limnol Oceanogr 61:1826–1838. https://doi.org/10.1002/lno.10339

Sun H, Han J, Zhang S, Lu X (2007) The impacts of '05.6' extreme flood event on riverine carbon fluxes in Xijiang River. ChSBu 52:805–812. https://doi.org/10.1007/s11434-007-0111-6

Teodoru CR, Nyoni FC, Borges AV, Darchambeau F, Nyambe I, Bouillon S (2015) Dynamics of greenhouse gases (CO_2, CH_4, N_2O) along the Zambezi River and major tributaries, and their importance in the riverine carbon budget. BGeo 12:2431–2453. https://doi.org/10.5194/bg-12-2431-2015

Tranvik LJ, Cole JJ, Prairie YT (2018) The study of carbon in inland waters-from isolated ecosystems to players in the global carbon cycle. Limnol Oceanogr Lett 3:41–48. https://doi.org/10.1002/lol2.10068

GHG UNESCO/IHA (2010) Greenhouse gas emissions related to freshwater reservoirs. World Bank Report 7150219

van Geldern R, Schulte P, Mader M, Baier A, Barth JAC (2015) Spatial and temporal variations of pCO_2, dissolved inorganic carbon and stable isotopes along a temperate karstic watercourse. HyPr 29:3423–3440. https://doi.org/10.1002/hyp.10457

Varol M, Li S (2017) Biotic and abiotic controls on CO_2 partial pressure and CO_2 emission in the Tigris River, Turkey. ChGeo 449:182–193. https://doi.org/10.1016/j.chemgeo.2016.12.003

Venkiteswaran JJ, Schiff SL, Wallin MB (2014) Large carbon dioxide fluxes from headwater boreal and sub-boreal streams. PLoS One 9:e101756. https://doi.org/10.1371/journal.pone.0101756

Wallin MB, Grabs T, Buffam I, Laudon H, Agren A, Oquist MG, Bishop K (2013) Evasion of CO_2 from streams—the dominant component of the carbon export through the aquatic conduit in a boreal landscape. Glob Chang Biol 19:785–797. https://doi.org/10.1111/gcb.12083

Wang F, Wang Y, Zhang J, Xu H, Wei X (2007) Human impact on the historical change of CO2 degassing flux in River Changjiang. Geochem Trans 8. https://doi.org/10.1186/1467-4866-8-7

Wang H, Liu Z, Zhang J, Sun H, An D, Fu R, Wang X (2010) Spatial an temporal hydrochemical variations of the spring-fed travertine-depositing stream in the Huanglong Ravine, Sichuang, SW China. Acta Carsologica 39:247–259

Wang X, He Y, Yuan X, Chen H, Peng C, Zhu Q, Yue J, Ren H, Deng W, Liu H (2017) pCO_2 and CO_2 fluxes of the metropolitan river network in relation to the urbanization of Chongqing, China. J Geophys Res Biogeosci 122:470–486. https://doi.org/10.1002/2016jg003494

Yang R, Chen B, Liu H, Liu Z, Yan H (2015) Carbon sequestration and decreased CO_2 emission caused by terrestrial aquatic photosynthesis: insights from diel hydrochemical variations in an epikarst spring and two spring-fed ponds in different seasons. Appl Geochem 63:248–260. https://doi.org/10.1016/j.apgeochem.2015.09.009

Yang R, Liu Z, Zeng C, Zhao M (2012) Response of epikarst hydrochemical changes to soil CO_2 and weather conditions at Chenqi, Puding, SW China. J Hydrol 468-469:151–158. https://doi.org/10.1016/j.jhydrol.2012.08.029

Yao G, Gao Q, Wang Z, Huang X, He T, Zhang Y, Jiao S, Ding J (2007) Dynamics of CO_2 partial pressure and CO_2 outgassing in the lower reaches of the Xijiang River, a subtropical monsoon river in China. Sci Total Environ 376:255–266. https://doi.org/10.1016/j.scitotenv.2007.01.080

Yuan D (1997) The carbon cycle in karst. Z Geomorphol 108(Suppl):91–102

Zeng F-W, Masiello CA (2010) Sources of CO_2 evasion from two subtropical rivers in North America. Biogeochemistry 100:211–225. https://doi.org/10.1007/s10533-010-9417-6

Zhang T, Li J, Pu J, Martin JB, Khadka MB, Wu F, Li L, Jiang F, Huang S, Yuan D (2017) River sequesters atmospheric carbon and limits the CO_2 degassing in karst area, southwest China. Sci Total Environ 609:92–101. https://doi.org/10.1016/j.scitotenv.2017.07.143

Zhao M, Liu Z, Li H-C, Zeng C, Yang R, Chen B, Yan H (2015) Response of dissolved inorganic carbon (DIC) and $\delta^{13}C_{DIC}$ to changes in climate and land cover in SW China karst catchments. GeCoA 165:123–136. https://doi.org/10.1016/j.gca.2015.05.041